Journal of Experimental Nanoscience
Publication details, including instructions for authors and subscription information:
http://www.informaworld.com/smpp/title~content=t716100757

Nanostructured thin layers of vanadium oxides doped with cobalt, prepared by pulsed laser ablation: chemistry, local atomic structure, morphology and magnetism

C. M. Teodorescu[a]; G. Socol[b]; C. Negrila[a]; D. Luca[c]; D. Macovei[a]
[a] Nanoscale Condensed Matter Physics Department, National Institute of Materials Physics, 077125 Magurele, Romania [b] Laser-Surface-Plasma-Interactions Laboratory, National Institute of Lasers, Plasma and Radiation Physics, 077125 Magurele, Romania [c] Department of Plasma Physics, Optics and Spectroscopy, 'Alexandru Ioan Cuza' University, 700506 Iasi, Romania

Online publication date: 17 December 2010

To cite this Article Teodorescu, C. M. , Socol, G. , Negrila, C. , Luca, D. and Macovei, D.(2010) 'Nanostructured thin layers of vanadium oxides doped with cobalt, prepared by pulsed laser ablation: chemistry, local atomic structure, morphology and magnetism', Journal of Experimental Nanoscience, 5: 6, 509 — 526
To link to this Article: DOI: 10.1080/17458081003671675
URL: http://dx.doi.org/10.1080/17458081003671675

Journal of Experimental Nanoscience
Vol. 5, No. 6, December 2010, 509–526

Taylor & Francis
Taylor & Francis Group

Nanostructured thin layers of vanadium oxides doped with cobalt, prepared by pulsed laser ablation: chemistry, local atomic structure, morphology and magnetism

C.M. Teodorescu[a]*, G. Socol[b], C. Negrila[a], D. Luca[c] and D. Macovei[a]

[a]*Nanoscale Condensed Matter Physics Department, National Institute of Materials Physics, Atomistilor 105b, 077125 Magurele, Romania;* [b]*Laser-Surface-Plasma-Interactions Laboratory, National Institute of Lasers, Plasma and Radiation Physics, Atomistilor 409, 077125 Magurele, Romania;* [c]*Department of Plasma Physics, Optics and Spectroscopy, 'Alexandru Ioan Cuza' University, Carol I Blvd. No. 11, 700506 Iasi, Romania*

(*Received 28 November 2008; final version received 2 February 2010*)

Cobalt-doped vanadium oxide thin layers prepared by pulsed laser ablation are investigated from the following points of view: (1) the chemical states by X-ray photoelectron spectroscopy (XPS), (2) the local atomic order by X-ray absorption fine structure at both vanadium and cobalt K-edges, (3) the morphology of the films by atomic force microscopy (AFM) and (4) the magnetic properties by magneto-optical Kerr effect (MOKE). The chemical composition of the host matrix was found to be close to VO_2 at the sample surface, with V_2O_3 in the bulk. Co ions are found near the surface in high ionisation states Co^{4+} (for the samples synthesised in a high vacuum condition, denoted by VO1), or with $Co^{(4-\delta)+}$ (for the samples synthesised in an oxygen atmosphere, denoted by VO2), whereas in the bulk, $Co^{1.5+}$ is obtained for VO1 and Co^{2+} is obtained for VO2. The AFM revealed nanoparticles with sizes 10–25 nm for VO1 samples, whereas a few bigger nanoparticles are observed for VO2 samples. The VO1 samples presented high coercitive fields with a relatively low saturation magnetisation at room temperature, superposed with a superparamagnetic component attributed to the observed nanoparticles, whereas the VO2 samples presented double-loop hysteresis curves, indicating the co-existence of two kinds of magnetic moieties with antiparallel coupling at zero applied field. The proposed two magnetic phases are Co-doped V_2O_3 and VO_2.

Keywords: vanadium oxide; pulsed laser deposition; X-ray photoelectron spectroscopy; X-ray absorption fine structure; atomic force microscopy; magnetic properties

1. Introduction

The synthesis of diluted magnetic semiconductors (DMS) is amongst the outstanding results of the past two decades in materials physics [1,2]. During recent years (2003–2008), DMS were successfully synthesised based on the (nonmagnetic) transition metal oxides (ZnO, TiO_2) doped with magnetic ions (Cr–Ni).

*Corresponding author. Email: teodorescu@infim.ro

ISSN 1745–8080 print/ISSN 1745–8099 online

DOI: 10.1080/17458081003671675
http://www.informaworld.com

In DMS, magnetic ordering is produced between isolated magnetic ions either (1) *via* the double exchange or RKKY interaction [3], where the interaction between magnetic ions is mediated by the charge carriers from the matrix or (2) by shallow donor electrons that form bound magnetic polarons, which overlap to create a spin-split impurity band [4]. Hence, the possibility of controlling magnetic ordering *via* the density of the charge carriers is provided by these systems. A wide range of applications may be foreseen starting with this phenomenon, such as induced ferromagnetism by light irradiation [1], DMS-based spintronic devices [2], ferromagnetism control *via* applied electric fields [5], and the possibility of domain wall displacement by varying the charge density [6]. A novel application was demonstrated in the possibility of ferromagnetic ordering by molecular adsorption at surfaces [7], using the carriers donated by molecular species for mediating ferromagnetism by double exchange.

This article deals with investigating the possibility of the synthesis of materials where magnetic ions are isolated in matrices which exhibit Mott-Hubbard metal–insulator transition (MIT) [8]. In this study, the chosen host materials are vanadium oxides, where MIT can be achieved at temperatures interesting for applications, in the range of 330–340 K for VO_2 and 150–160 K for V_2O_3 [9,10]. This transition temperature may also be tuned by varying the relative vanadium–oxygen composition ratio. Recently, ultrafast light-induced MIT transitions were reported in VO_2 thin layers [11]. Also, the first explorations revealed interesting magnetic properties, such as uniaxial magnetic anisotropy, or persistent orbital currents on materials starting with doped vanadium oxide [12]. The practical realisation of such materials would open the controlling possibilities of the occurrence of ferromagnetic ordering through the strong variation of charge density following the Mott-Hubbard transition from the insulating to the metal state. Also, according to Ref. [11], one might expect that such a transition may be very fast, therefore offering the possibility of ultrafast magnetic switches with a wide range of technological applications.

2. Experimental

The materials were synthesised by pulsed laser deposition (PLD) in the National Institute of Lasers, Plasma and Radiation Physics, Magurele. The targets were prepared by sintering a mixture of vanadium oxide (VO_2) and cobalt in various proportions. The PLD was performed by using an excimer laser (KrF) at the value of 9 J/cm^2, in a controlled atmosphere: (1) in vacuum (10^{-5} mbar $= 10^{-3}$ Pa) and (2) in an oxygen atmosphere (from 10^{-3} mbar $\approx 10^{-1}$ Pa to 10^{-1} mbar ≈ 10 Pa). The depositions were realised on a single crystal Si(0 0 1) and quartz SiO_2(0 0 1). The substrates were heated during deposition in order to improve crystallinity and to avoid the formation of macroscopic droplets. The sample thicknesses were 1 μm (±8%), as determined from the number of laser pulses. The system is calibrated periodically by profilometric measurements, so as to determine the equivalent thickness corresponding, in average, to a given number of pulses.

The X-ray photoelectron spectroscopy (XPS) was performed by using a VG-ESCA MK II installation (upgraded with a Specs X-ray gun and electron flood gun and with a Pfeiffer quadrupole mass spectrometer) in the National Institute of Materials Physics (NIMP), Magurele. The X-ray gun was operated with Al K_α radiation (1486.7 eV). The photoelectrons were detected using a hemispherical electron analyser with 100 mm radius

operating at a pass energy of 100 eV for survey spectra and at 50 eV for individual core level spectra. The samples were not sputtered to remove the contamination layer prior to measurements as it was demonstrated that sputtering affects the stoichiometry of the samples (the samples are oxygen depleted) [13] and this point is crucial for our investigations.

Magneto-optical Kerr effect (MOKE) measurements at room temperature were performed in NIMP Magurele by using a AMACC Anderberg & Modéer Accelerator MiniMOKE system with He–Ne laser radiation. The X-ray absorption fine structure (XAFS: extended X-ray absorption fine structure EXAFS and X-ray absorption near-edge structure XANES) measurements were performed at the Doris storage ring facility in Hasylab, Hamburg, Germany (A1 beamline), by using a Si(1 1 1) double crystal monochromator. The measurements on Co-doped vanadium oxide thin layers were performed in fluorescence mode by using a Si–Li detector and selecting the channels corresponding to the fluorescent radiation of interest (Co or V K_α). For consistent data interpretation, standards of metallic Co and V, of Co(II)O and of vanadium oxides: V_2O_5, VO_2, V_2O_3 (Aldrich) were measured in the same run, in the transmission mode on a 5 μm Co foil for the metal and of pressed pellets of powders mixed with cellulose for the oxides. The atomic force microscopy (AFM) was performed in the University of Iasi by using home-made equipment, operating in tapping mode.

3. Results and discussion

Although several investigations were performed, we mainly discuss the differences presented by the samples prepared in high vacuum conditions (10^{-5} mbar $\approx 10^{-3}$ Pa) and in an oxygen atmosphere (oxygen pressure of 10^{-3} mbar ≈ 0.1 Pa), with a nominal Co concentration of 10% in the target. All the samples discussed here were deposited on the substrate held at 450°C.

3.1. *X-ray photoelectron spectroscopy*

Figure 1 presents the survey of XPS spectra on two samples (VO1, synthesised at 10^{-5} mbar and VO2, prepared at 10^{-3} mbar). One notices the presence of V, O and Co photoelectron and Auger electron signals and of carbon contamination from the inherent contamination layer. A first observation is that the carbon contamination visibly decreases when the synthesis is performed in an oxygen atmosphere; at the same time, in this case, the Co 2*p*, V 2*p* and O 1*s* signals show a noticeable increase.

One also observes the presence of Cu and, for the VO1 sample, of Zn. This is connected to the copper or brass plates on which the samples were mounted. The most intriguing result here is the presence of the N 1*s* level in both samples. Usually, this level does not come from the contamination layer. Therefore, it may be inferred that in this case nitrogen is present in the sample itself, integrated by the sputtering procedure as a possible contaminant of the gas inlet. The integral amplitude of this level is $4.5 \pm 0.5\%$ from the oxygen level. Therefore, the synthesised samples are nitrogen doped from the very moment of preparation.

Figure 2 presents the V 2*p* and O 1*s* core level electron distribution curves (EDC). The spectra were deconvoluted by using the Voigt profiles accounting for the Lorentzian

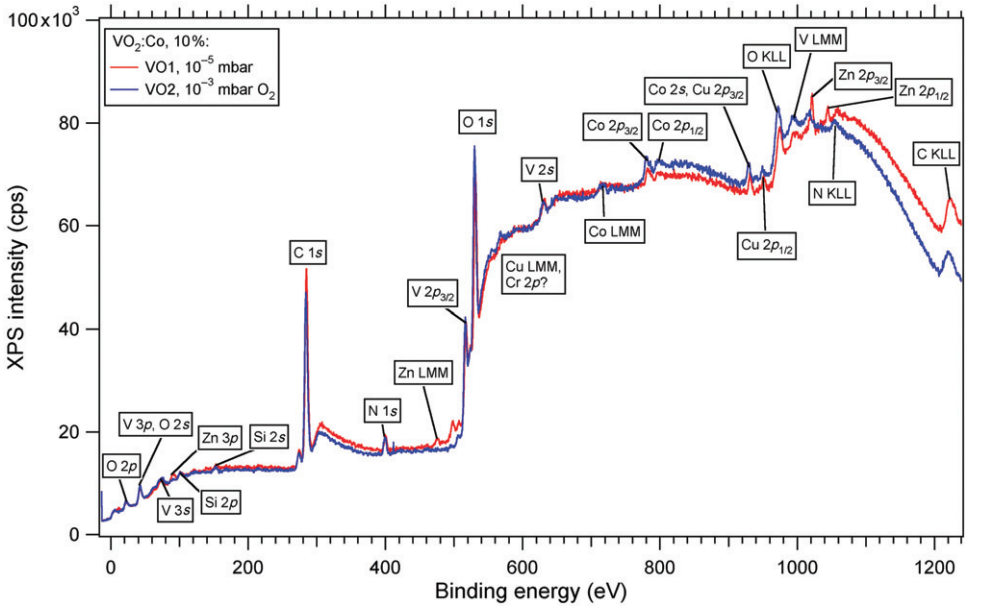

Figure 1. Survey XPS scan of the two samples VO1 and VO2, synthesised at different values of the oxygen pressure.

widths, which originate from (1): the natural width of the X-ray excitation line and (2): from the inner-level core hole width – and form a Gaussian width, assumed to originate from the electron energy analyser. The analytical approximation used is taken from Ref. [14]. A Voigt profile obtained from the convolution of a Lorentzian line shape with full width at half maximum (FWHM) W_L and of a Gaussian line shape with FWHM W_G will be denoted by $F(W_L, W_G, x)$. Each core level also has an associated background due to the inelastic scattering processes of the photoelectrons. This background is simulated with an integral (primitive of the Voigt function) of step unity $P(W_L, W_G, x) = \int_{-\infty}^{x} F(W_L, W_G, x')\mathrm{d}x'$, which is also parameterised in Ref. [13]. Hence, each core level situated at the binding energy, BE, is simulated by a combination of the Voigt profile and its integral $G(W_L, W_G, \mathrm{BE}, \mathrm{IB};\ x) = F(W_L, W_G, x - \mathrm{BE}) + \mathrm{IB} \times P(W_L, W_G, x - \mathrm{BE})$, where IB represents the inelastic background coefficient. The use of separate inelastic background coefficients for different core levels allows one to investigate whether the atoms responsible for the respective components are situated in the bulk or at the sample surface (in the latter case IB yielding a very low value), as was reported the first time in Ref. [15]. A correct deconvolution is obtained by using only one doublet for the V 2*p* level ($2p_{3/2}$ and $2p_{1/2}$ core levels, separated by the spin-orbit splitting SO (V 2*p*), whose amplitude ratio is called the 'branching ratio', *BR*) and two singlets for the O 1*s* level, which are apparent also from the asymmetry of the O 1*s* lineshape (Figure 2). The origin of these two components is straightforward: the lower binding energy component (530.6–530.7 eV) represents oxygen from the bulk of the sample, whereas the higher binding energy component (532.3–532.5 eV) corresponds to the oxygen from the outermost contamination layer in C=O, C–OH, etc. [16]. Also, we allowed a considerable

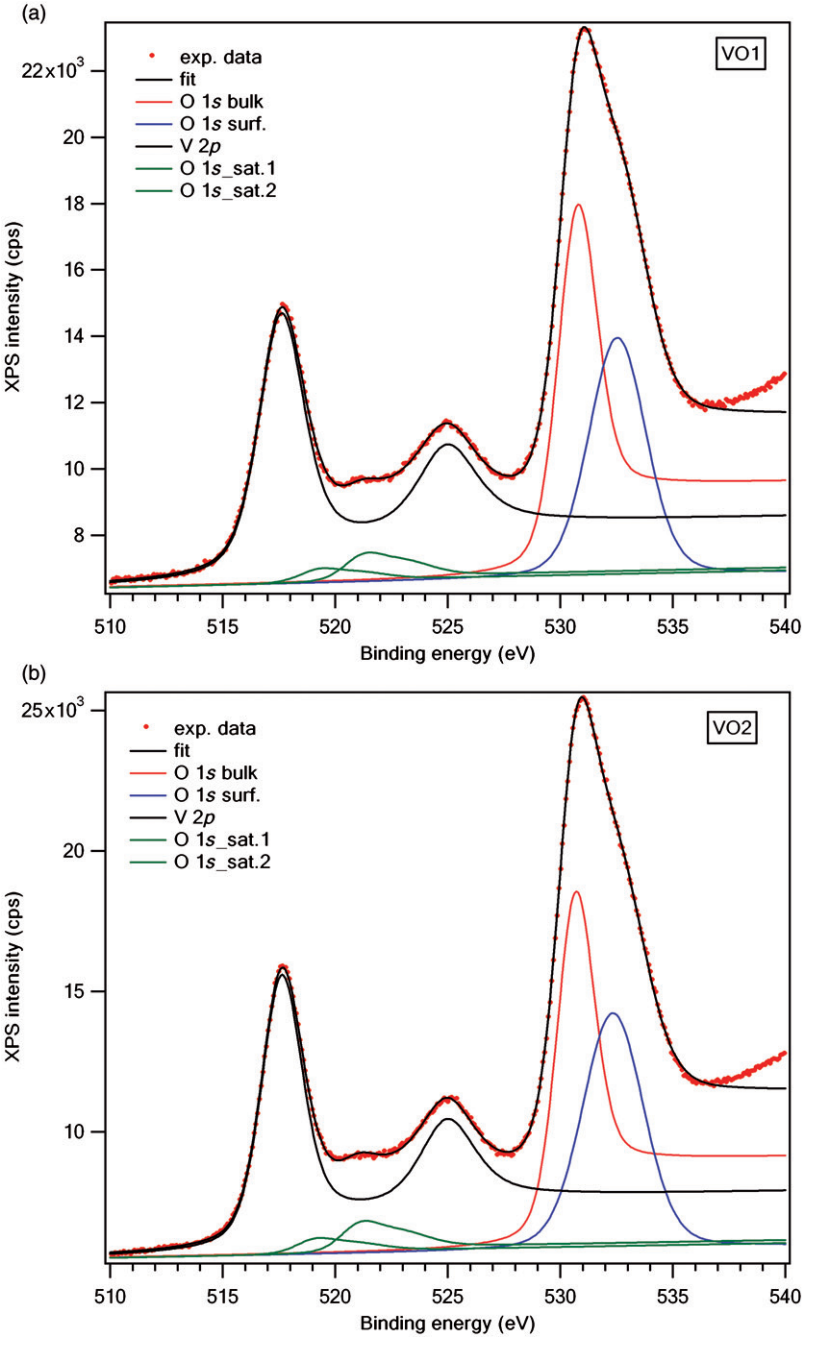

Figure 2. V 2*p* and O 1*s* EDC on samples VO1 (a) and VO2 (b), together with deconvolutions using Voigt profiles for the XPS lines and Voigt integrals for the inelastic backgrounds.

increased value of the Gaussian width for the contamination component, to account for the variety of chemical states of surface oxygen from the contamination layer. At the same time, at the V 2*p* doublet, the same Gaussian width was used for both components (being also the same as for the O 1*s* component, since it is mainly related to the electron energy analyser), but we allowed an increased value of the Lorentzian width for the $2p_{1/2}$ component, compared with the $2p_{3/2}$ component. The origin of the increased width of the higher binding energy component is the shortening of the lifetime of the core hole (denoted as$2p_{1/2}^{-1}$) due to the opening of Coster–Kronig de-excitation channels ($2p_{1/2}^{-1}$ $2p_{3/2} \rightarrow 2p_{1/2}$ $2p_{3/2}^{-1}$ $v^{-1}f$, i.e. the $2p_{1/2}$ hole is filled by a $2p_{3/2}$ electron and the excess energy is taken by a valence electron *v* escaping in a final free state *f*) [15].

The deconvolution problem is further complicated by the intermixing of the O 1*s* satellites due to the excitation with Al $K_{\alpha 3,4}$ in the V 2*p* region. This satellite is simulated by fitting the O 1*s* components with the same parameters, however, energy shifted by the amounts $\Delta E_s^{(1)} \sim 9.5$–$9.8$ eV and $\Delta E_s^{(2)} \sim 11.5$–$11.8$ eV towards lower binding energies and multiplied by a factor *p*. Globally, the total fitting function is written as

$$Fit_{XPS}(\vec{c}; x) = V_{2p}(\vec{c}; x) + O_{1s}^{\text{bulk}}(\vec{c}; x) + O_{1s}^{\text{surface}}(\vec{c}; x) + O_{1s}^{\text{satellite}}(\vec{c}; x) + b + s \times x \quad (1)$$

with $\vec{c}$ being the vector of fitting coefficients, *b* the baseline and *s* an admitted small slope of the spectrum. The separate components are written as:

$$\begin{aligned} V_{2p}(\vec{c}; x) = \frac{\text{IA}(V2p)}{\text{BR}(V2p)+1} \{ &\text{BR}(V2p) \times G\big[W_{\text{L}}(V2p_{3/2}), W_{\text{G}}(V2p + O1s_{\text{bulk}}), \\ &\times \text{BE}(V2p_{3/2}), \text{IB}(V2p); x\big] + G\big[W_{\text{L}}(V2p_{1/2}), W_{\text{G}}(V2p + O1s_{\text{bulk}}), \\ &\times \text{BE}(V2p_{3/2}) + \text{SO}(V2p), \text{IB}(V2p); x\big]\} \end{aligned} \quad (2)$$

$$\begin{aligned} O_{1s}^{\text{bulk}}(\vec{c}; x) = \text{IA}(O1s_{\text{bulk}}) \times G[&W_{\text{L}}(O1s_{\text{bulk+surface}}), W_{\text{G}}(V2p + O1s_{\text{bulk}}), \\ &\times \text{BE}(O1s_{\text{bulk}}), \text{IB}(O1s_{\text{bulk}}); x] \end{aligned} \quad (3)$$

$$\begin{aligned} O_{1s}^{\text{surface}}(\vec{c}; x) = \text{IA}(O1s_{\text{surface}}) \times G[&W_{\text{L}}(O1s_{\text{bulk+surface}}), W_{\text{G}}(O1s_{\text{surface}}), \\ &\times \text{BE}(O1s_{\text{surface}}), \text{IB}(O1s_{\text{surface}}); x] \end{aligned} \quad (4)$$

$$\begin{aligned} O_{1s}^{\text{satellite}}(\vec{c}; x) = p \times \Bigg[&O_{1s}^{\text{bulk}}\left(\vec{c}; x - \Delta E_s^{(1)}\right) + O_{1s}^{\text{surface}}\left(\vec{c}; x - \Delta E_s^{(1)}\right) \\ &+ \frac{O_{1s}^{\text{bulk}}(\vec{c}; x - \Delta E_s^{(2)}) + O_{1s}^{\text{surface}}(\vec{c}; x - \Delta E_s^{(2)})}{2} \Bigg]. \end{aligned} \quad (5)$$

In the last equations, IAs represent integral amplitudes of the 2*p* doublet or 1*s* individual lines. The fixed parameters were the branching ratio between the V 2*p* levels BR(V 2*p*) = 2 and also the energy difference between the two satellite components of the O 1*s*: $\Delta E_s^{(2)} - \Delta E_s^{(1)} = 2.0$ eV. In total, there were 19 fitting parameters. Seventeen of these fitting parameters are listed in Table 1, the remaining two being the baseline *b* and the slope *s*, without physical significance. The separate components resulting from Equations (2)–(5) are also represented in Figure 2. One immediate result was that the

Table 1. Results of the deconvolutions of the XPS spectra (V 2*p* and O 1*s*).

Sample	Units	VO1	VO2
Fitting parameter			
BE (V $2p_{3/2}$)	eV	517.583 ± 0.005	517.61 ± 0.005
IA (V 2*p*)	kcps × eV	34.95 ± 0.12	37.65 ± 0.13
SO (V 2*p*)	eV	7.37 ± 0.007	7.35 ± 0.009
W_L (V $2p_{3/2}$)	eV	1.15 ± 0.09	0.89 ± 0.08
W_L (V $2p_{1/2}$)	eV	2.27 ± 0.21	2.03 ± 0.19
W_G (V $2p$ + O $1s_{bulk}$)	eV	1.68 ± 0.18	1.63 ± 0.18
IB (V 2*p*)	$0.01\,eV^{-1}$	4.9 ± 0.2	5.2 ± 0.3
BE (O $1s_{bulk}$)	eV	530.73 ± 0.004	530.64 ± 0.004
IA (O $1s_{bulk}$)	kcps × eV	23.96 ± 0.09	26.12 ± 0.11
IB (O $1s_{bulk}$)	$0.01\,eV^{-1}$	11.3 ± 0.8	12.0 ± 0.9
W_L (O $1s_{bulk+surface}$)	eV	0.65 ± 0.02	0.62 ± 0.02
BE (O $1s_{surface}$)	eV	532.54 ± 0.01	532.34 ± 0.01
IA (O $1s_{surface}$)	kcps × eV	24.59 ± 0.11	30.83 ± 0.15
IB (O $1s_{surface}$)	$0.01\,eV^{-1}$	0 ($<10^{-9}$)	0 ($<10^{-4}$)
W_G (O $1s_{surface}$)	eV	2.64 ± 0.03	2.86 ± 0.05
ΔE_s (O 1*s* satellite)	eV	9.55 ± 0.06	9.62 ± 0.06
p (O 1*s* satellite)	%	6.14 ± 0.24	6.71 ± 0.28
Co 2*p* estimate (without fitting)			
BE (Co $2p_{3/2}$)	eV	~782.1	~782.0
IA (Co $2p_{3/2}$)	kcps × eV	~3.2	~6.3
FWHM (Co $2p_{3/2}$)	eV	~4.70	~4.62
IB (Co $2p_{3/2}$)	0.01 eV	~9	~6

Notes: For Co 2*p*, we only give an estimate, without deconvolution. BE represents binding energies, IA the integral peak amplitudes, SO the spin-orbit splitting of the V $2p_{3/2}$–$2p_{1/2}$ the core levels, IB the inelastic background ratio. W_L the Lorentzian FWHM from the Voigt profile and W_G the Gaussian FWHM. For the Co 2*p*, we estimated only the total FWHM from the raw data. Also, the parameters used for the satellite contribution from the O 1*s* (ΔE_s and *p*) are given. See Equation (1) for the significance of all parameters.

second component in the oxygen 1*s* spectrum has a very low inelastic background. Therefore, oxygen atoms located at the surface (the contamination layer) are responsible for this component, as expected and as reported previously for titanium dioxide samples [15]. The quality of the fitting is good enough; errors in the determination of parameters are determined by performing many (~several hundred) fittings with randomly input parameters and by measuring the spreading of the resulting values for the parameters.

In order to derive the vanadium ionisation states, we have also performed a complete analysis of the reported data in the literature.

Figure 3 shows the analysis of the V 2*p* data from different vanadium oxides, as vanadium exist in several oxidation states, from (II) to (V). The data are extracted from Ref. [17]. We also added data for vanadium metal, also from Ref. [17]. By comparing these data with the experimental BE derived from the deconvolutions presented in Figure 2 and synthesised in Table 1, one may infer the presence of vanadium in a (+5) ionisation state, therefore by forming the compound V_2O_5. This result is a bit deceiving, since this compound does not present a Mott-Hubbard transition at a convenient temperature.

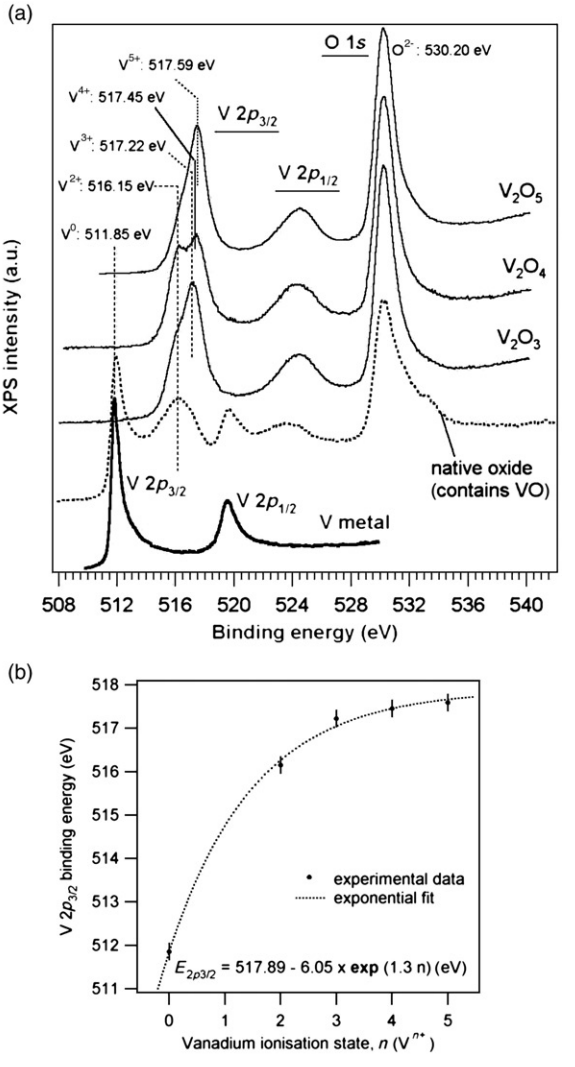

Figure 3. V 2*p* and O 1*s* EDC on several vanadium oxides: (a) XPS data; (b) dependence of the derived V $2p_{3/2}$ binding energy on the vanadium ionisation state. The fit is an empirical exponential function.

There are, however, two comments worth pointing out (1) the (+4) state cannot be precluded, since its BE for vanadium core levels (517.45 eV) is close enough to its value for (+5) (517.69 eV) and (2) we may also anticipate that this conclusion is valid for the uppermost ~15–20 Å from the sample surface, owing to the photoelectron inelastic mean free path [18].

Figure 4(a) presents the Co 2*p* EDC for both samples. Figure 4(b) synthesises the existing data for the Co $2p_{3/2}$ binding energy from the literature for cobalt metal [19] and for cobalt in various stable oxides: CoO [20], Co_3O_4 [21], Co_2O_3 [22]. The existing data were fit with a straight line, which was extrapolated for the higher binding energies

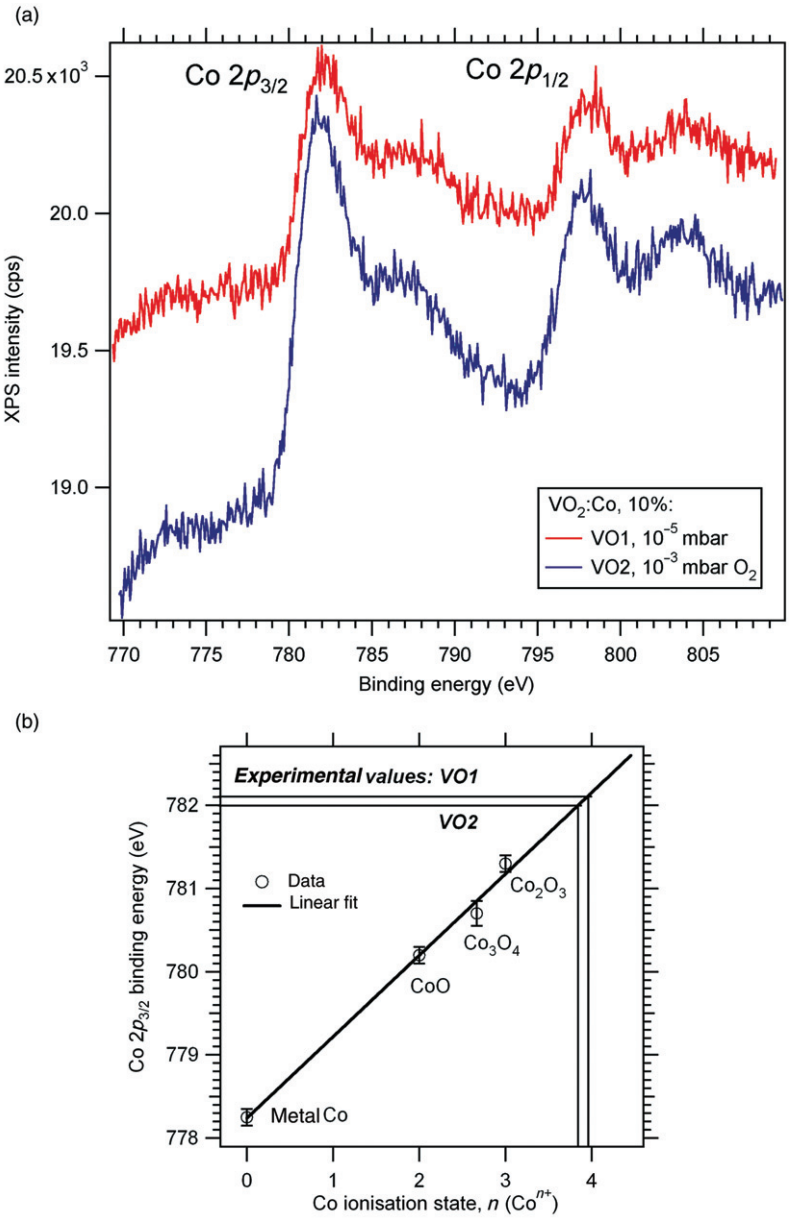

Figure 4. (a) Co 2*p* EDC for VO1 and VO2; (b) Co $2p_{3/2}$ binding energy dependence on the cobalt ionisation state – data from Refs. [18–21]. This dependence was empirically fitted by a straight line.

observed in the measured spectra. This allows one to infer that in our cobalt-doped vanadium oxides, cobalt is found in an ionisation state close to (+4): more precisely, we obtain Co^{4+} for VO1 and $Co^{\sim 3.85+}$ for VO2. Hence, the cobalt ionisation state seems to be a bit lower when the sample is prepared in an oxygen atmosphere.

The core-level integral intensities, analysed by using the atomic sensitivity factors (ASF) tabulated by Wagner et al. [23] (ASF = 0.66 for O 1*s*, 0.42 for N 1*s*, 1.95 for V 2*p* and 2.5 for Co $2p_{3/2}$), enabled us to infer the nominal composition (atomic ratios Co:V:O) of (1.28:17.92:36.30) for sample VO1 (10^{-3} Pa) and of (2.52:19.31:39.57) for sample VO2 (0.1 Pa). Consequently, the compounds close to $(Co_xV_{1-x})O_{2-\delta}$ (with $x \approx 7\%$ and $\delta \approx 11\%$ for VO1 and $x \approx 12\%$, $\delta \approx 19\%$ for VO2) are obtained from the intensity analysis. This questions the previous assumption that a compound close to V_2O_5 is obtained, as derived from binding energy considerations. On the other hand, from Figure 3(b) it follows that the $2p_{3/2}$ BE in VO_2 and in V_2O_5 are nearly the same and so globally we might infer that the samples are VO_2 doped with cobalt, with a slight oxygen deficit of oxygen atoms which could be substituted by nitrogen. From the survey of XPS scans, the nitrogen atomic content may be estimated to be $7.1 \pm 0.8\%$ when taking into account the atomic sensitivity factors. We may then conclude that there is a good agreement between the binding energy and the line intensity determination of the chemical state.

However, it is worth noting that the presence of oxygen vacancies may favour the occurrence of ferromagnetism, *via* the mechanisms discussed in Ref. [4].

3.2. *X-ray absorption near-edge spectroscopy*

Figure 5(a) presents the V K-edge XANES on the three oxides investigated: V_2O_3, VO_2 and V_2O_5, whereas Figure 5(b) presents the V K-edge XANES on the PLD-prepared samples VO1 and VO2. From the analysis of the pre-edge region, where dipole forbidden transitions $1s \rightarrow 3d$ manifest [24], one derives the average number of 3*d* vacancies and hence the vanadium oxidation state. From Figure 5(a) and (b), different ionisation states may be inferred for vanadium, namely (+3) for VO1 and around (+3.5) for VO2, which corresponds to vanadium (III) or V_2O_3 for sample VO1 and to something like V_4O_7 for sample VO2. Nevertheless, both compositions are between V_2O_3 and VO_2, which are the compounds exhibiting MIT. The latter compound could also be described as a kind of mixture, such as $(2 \times VO_2 + V_2O_3)$ or $(3 \times VO_2 + VO)$. A compound similar to VO (i.e. V(II)) is actually identified in the vanadium native oxide on surfaces in a vacuum (Figure 3) and was recently noted for thin films prepared by using a plasma atomisation source [25].

Therefore, the oxygen deficit δ defined when the XPS data were discussed the results larger from XANES than from the XPS data analysis, especially for VO1: $\delta \sim 0.5$ for VO1 (instead of 0.11); for VO2, the XANES data are more in agreement with the XPS data: $\delta \sim 0.25$ from XANES and 0.19 from XPS. Here one has to take into account that the investigated depth is around 1–2 nm in XPS owing to the photoelectron escape depth [18]. Whereas in X-ray absorption recorded in fluorescence mode, the investigated depth is in several hundreds of nanometre (up to the micrometre range). Therefore, although at the surface a compound close to vanadium dioxide ($V_2O_4 \equiv VO_2$) is formed, by varying the oxygen pressure one may succeed in synthesising vanadium oxides with V in the lower ionisation states, such as mostly vanadium sesquioxide, V_2O_3 or V_4O_7, compounds susceptible to exhibiting a Mott–Hubbard transition at temperatures close to or even below the room temperature.

The Co K-edge XANES is represented in Figure 5(c). The Co spectrum is not similar to that of the cobalt (II) oxide. However, one may derive the cobalt ionisation state by

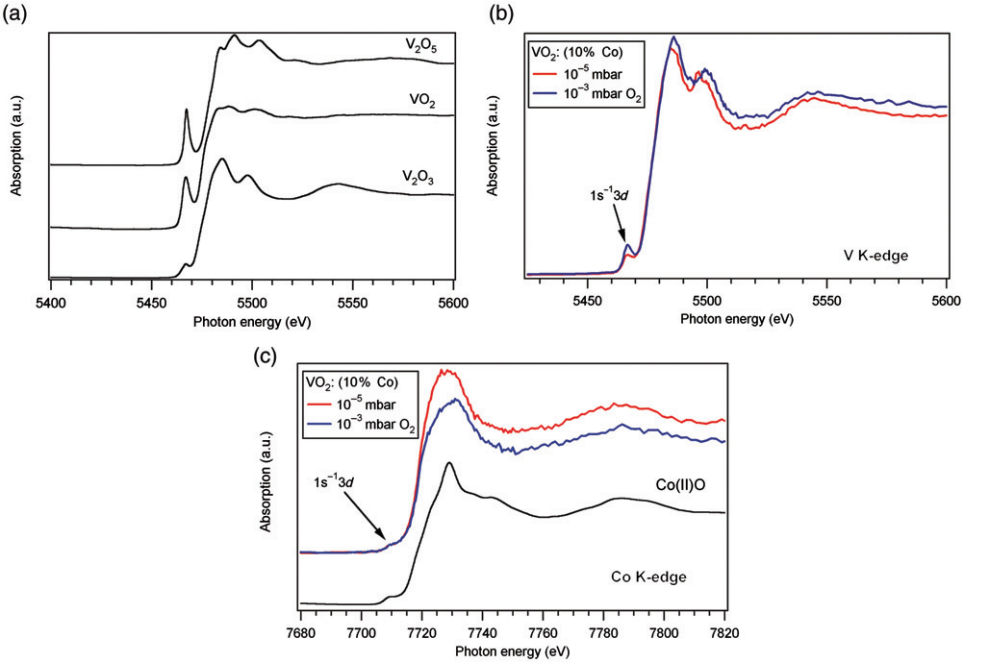

Figure 5. K-edge X-ray absorption near-edge structure (XANES): (a) vanadium K-edge spectra recorded on standard powders of V_2O_5, VO_2 and V_2O_3; (b) vanadium K-edge spectra recorded on Co-doped vanadium oxide prepared by PLD; (c) cobalt K-edge spectra on the Co-doped vanadium oxides, compared with the spectrum of standard Co(II) oxide.

assuming that the pre-edge peak ($1s \rightarrow 3d$ transitions [24]) is proportional to the average number of $3d$ vacancies. By computing the integral of this pre-edge peak and normalising to the amplitude of the absorption threshold an average ionisation state of around (+1.5) is obtained for the sample VO1 (prepared in vacuum) and around (+2) for the sample VO2 (prepared in an oxygen atmosphere). This result again contradicts the obtained ionisation states for cobalt from XPS, which were close to (+4). Again, one may invoke the different surface sensitivity of both techniques: at the sample surface, cobalt is found in higher ionisation states (close to 4+), as derived by XPS, whereas in the bulk, cobalt is found in lower ionisation states (close to 2+).

3.3. *Extended X-ray absorption fine structure spectroscopy*

Figure 6(a) represents the EXAFS functions $\chi(k) = \mu(k)/\mu_0(k) - 1$ (μ is the X-ray absorption coefficient, μ_0 the unstructured (atomic) absorption and k the photoelectron wave vector, whose kinetic energy is $\hbar^2k^2/(2m)$), weighted by the square of the photoelectron wave vector, k^2. The represented spectra were measured at the Co and V K-edges (7709 eV and 5465 eV, respectively) for the samples of interest, together with the spectra of standards to be compared with: metal Co and metal V, vanadium oxides V_2O_3, VO_2 and V_2O_5, and Co(II) oxide. Figure 6(b) represents the Fourier transforms of the functions $k^2\chi(k)$, by using a Hanning window [26].

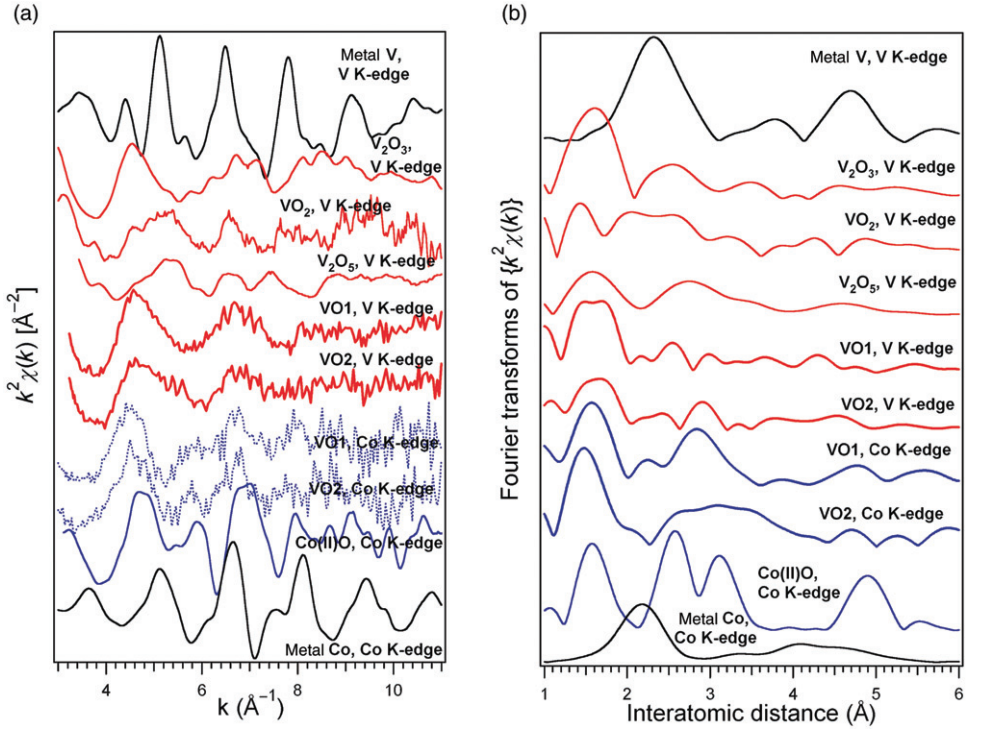

Figure 6. Extended X-ray absorption spectra of: (1) metal vanadium, recorded at the V K-edge; (2) standard vanadium oxides: V_2O_3, VO_2 and V_2O_5, recorded at the V K-edge; (3) PLD-prepared Co-doped vanadium oxide thin layers VO1 and VO2, at both V and Co K-edges; (4) standard Co(II) oxide, at the Co K-edge; (5) metal Co, Co K-edge. (a) Represents the oscillatory EXAFS functions, whereas (b) represents their Fourier transforms.

The most important conclusion of the EXAFS data is that the vanadium K-edge EXAFS looks quite similar to the spectrum recorded on V_2O_3, for both samples VO1 and VO2. This result agrees completely with the XANES result. Another conclusion is that the cobalt K-edge spectrum does not resemble that of the cobalt (II) oxide. Although the statistics of this spectrum does not enable accurate determinations, at least the spectrum of the VO1 sample (Figure 6(a)) and its Fourier transform (Figure 6(b)), are quite similar to the vanadium K-edge spectrum in V_2O_3. Consequently, sample VO1 may be regarded as being composed by cobalt-substituting vanadium in V_2O_3. For sample VO2, the interpretation of the cobalt EXAFS data is not that straightforward. Nevertheless, the Fourier transform of the Co K-edge spectrum may be regarded as an intermediate between the Fourier transforms of the vanadium K-edge in V_2O_3 and in VO_2. Consequently, a local cobalt environment similar to vanadium in these two compounds may be proposed for this sample.

3.4. *MOKE investigations*

Figure 7 presents the MOKE hysteresis loops obtained on both samples. Sample VO1 exhibits a strong (super) paramagnetic behaviour, superposed with a weak ferromagnetic

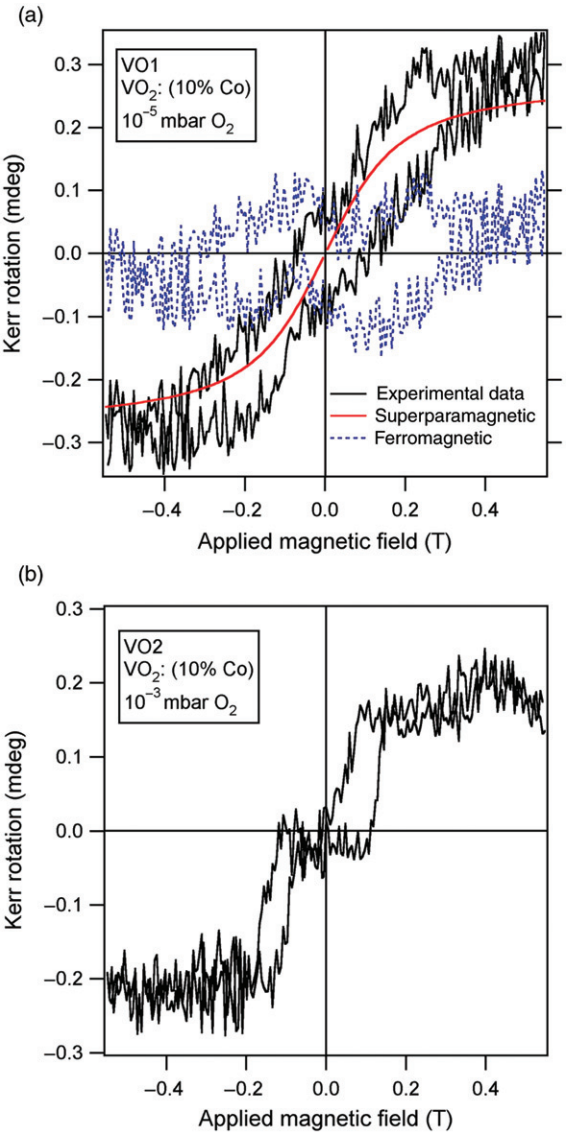

Figure 7. MOKE measurements on (a) sample VO1, prepared in vacuum (10^{-3} Pa); (b) sample VO2, prepared in oxygen atmosphere (0.1 Pa). In (a), the separate superparamagnetic (simulated) and ferromagnetic (difference experimental – superparamagnetic) contributions are plotted separately.

component with a strong coercitive field (0.33 ± 0.15 T), suggesting the presence of two magnetic phases: one which is superparamagnetic (this might originate from cobalt-vanadium oxide aggregates), the other being a kind of DMS (cobalt ions interacting by double exchange). The hysteresis cycle obtained for sample VO2 suggests the occurrence of a strong anisotropy, superposing a ferromagnetic and an antiferromagnetic phase, possibly interacting by exchange bias [12,27].

The hysteresis curve of sample VO1 was simulated with a superparamagnetic component, described by the Brillouin function [28]:

$$B_J\left(\frac{g\mu_B\mu_0 \mathrm{JH}}{k_B T}\right) = \frac{2J}{2J+1}\cot\left(\frac{2J}{2J+1}\frac{g\mu_B\mu_0 \mathrm{JH}}{k_B T}\right) - \frac{1}{2J+1}\cot\left(\frac{g\mu_B\mu_0 \mathrm{JH}}{(2J+1)k_B T}\right). \quad (6)$$

The best fit is obtained with a value of $J = 3000 \pm 200$ Planck units if we assume Co^{2+} ($S = 3/2$) corresponds to around 2000 Co ions in average per magnetic nanoparticle. For Co^{+} ($S = 1$), the number of cobalt ions per nanoparticle is 3000 and for Co^{3+} ($S = 2$), 1500 cobalt ions are computed for a nanoparticle. Regarding to the XPS results on cobalt concentration, assuming that these results hold for the superparamagnetic nanoparticles, for a 7% atomic cobalt concentration in VO_2, implies that the total number of atoms in a nanoparticle (cobalt + vanadium + oxygen) would be between $1500 \times 3/0.07$ and $3000 \times 3/0.07$ = between 6.4×10^4 and 1.3×10^5 atoms. By considering an average metal (cobalt or

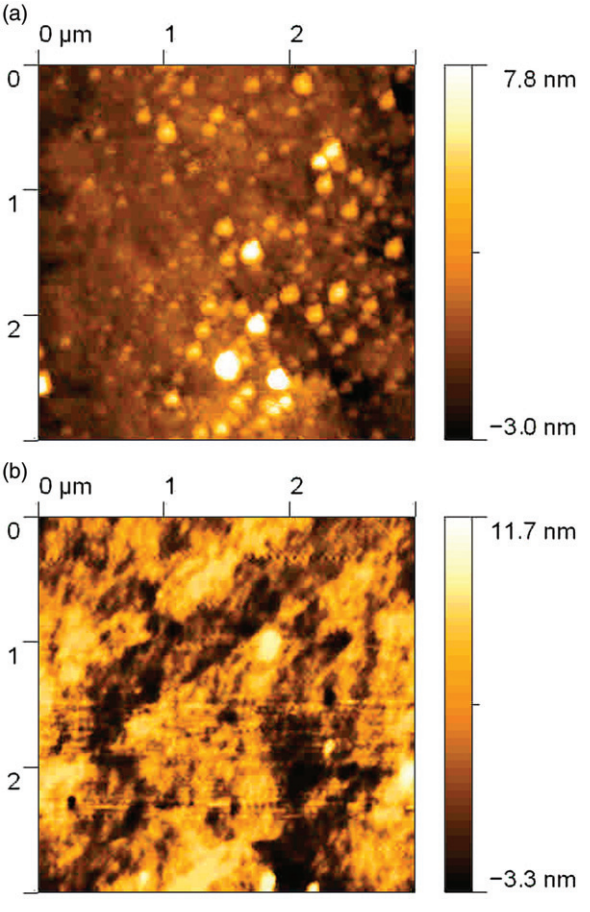

Figure 8. AFM images (a) on sample VO1, synthesised in a vacuum (10^{-3} Pa); (b) on sample VO2, synthesised in an oxygen atmosphere (0.1 Pa).

vanadium) – oxygen distance of 2.1 Å, which is an average obtained from Co and VO_2, and that the total number of atoms that are forming spherical nanoparticles, the diameters of these nanoparticles would range between 10.7 and 13.4 nm. Indeed, we will see that such nanoparticles are detected by AFM.

The remaining ferromagnetic component for sample VO1 has a behaviour foreseeing the magnetic signal for sample VO2. In the latter case, the hysteresis cycle suggests the presence of two magnetic phases, which at zero applied field are antiferromagnetic ordered. As soon as a relatively weak field (~0.1 T) is applied, the two phases are ordered parallel and this produces the observed hysteresis cycles. Such behaviour was also seen in Fe layers with different anisotropies, in structures such as Fe/Ag/Fe/GaAs(0 0 1) [27]. A similar behaviour was also observed in Fe/InAs(0 0 1), where the interface layer has a different magnetic moment and anisotropy compared with the uppermost Fe layer [29]. A tentative assignment of the two magnetic phases will be discussed in Section 4.

3.5. *Atomic force microscopy*

The AFM images are presented in Figure 8. In the case of the sample VO1, synthesised in a vacuum, a relatively high rugosity (1.61 nm rms) and the occurrence of nanoparticles with sizes between 10 and 25 nm are observed. This result is in line with the observation of the superparamagnetic behaviour in this sample. In the case of the sample VO2, synthesised in an oxygen atmosphere, larger nanoparticles are detected (which might explain the absence of the superparamagnetic behaviour in the magnetic hysteresis) and the rugosity decreases at 0.84 nm rms. We may also point out another result obtained within this study, namely that with the increase of oxygen pressure during the PLD synthesis, coalescing nanoparticles are observed by AFM; however, it seems that from the magnetic point of view, even for VO2 sample the nanoparticles had coalesced into the two magnetic phases producing the hysteresis cycle of Figure 7(b).

4. Conclusion

This article presented a first report on a combined study of samples formed by magnetic ions embedded in a Mott–Hubbard material (vanadium oxide), by correlating reactivity and chemical composition measurements (XPS) with electronic structure (XANES), local atomic order (EXAFS) magnetism (MOKE) and morphology (AFM). We identified different ionisation states of vanadium and cobalt between the surface and bulk of materials; the bulk composition seems to be tunable through preparation parameters. Promising ferromagnetic behaviour is observed, also dependent on the preparation conditions and these data were correlated with observations by AFM.

The main results obtained in this study are (1) a different composition between the sample surface and the bulk, especially for the sample synthesised at low pressure; (2) a clear evidence of the possibility of the synthesis of vanadium sesquioxide V_2O_3 in the bulk; (3) an almost clear evidence of substitutional insertion of cobalt on vanadium sites in the bulk; (4) room temperature ferromagnetism, however combined with the existence of superparamagnetism in the samples synthesised in a vacuum, and with the co-existence of two magnetic phases, antiferromagnetic aligned in the zero field, for samples synthesised in an oxygen atmosphere and (5) a clear correlation between the size

of magnetic nanoparticles observed by AFM and the derived total magnetic moments per nanoparticles from the analysis of the superparamagnetic behaviour.

The distinct magnetic behaviour of the VO_2 sample with the two magnetic phases compensating at zero applied field may be connected to the approximate stoichiometry derived by XANES for the bulk as $V_4O_7 \approx 2 \times VO_2 + V_2O_3$. Both vanadium dioxide and vanadium sesquioxide doped with cobalt present ferromagnetism at room temperature. The reciprocal antiferromagnetic alignment of these two phases needs, however, further experimental investigation by Kerr microscopy of magnetic force microscopy.

Problems not yet elucidated, which are currently under investigation, are: (1) the precise determination of the two magnetic phases which produce a hysteresis cycle such as from Figure 7(b). Up to now, we may propose that, since the Co K-edge EXAFS for this sample seemed to indicate the co-existence of cobalt substituting vanadium in VO_2 and V_2O_3 and also the V K-edge XANES indicated a global composition of V_4O_7, which may be written as $(2 \times VO_2 + V_2O_3)$, it could be possible that the two magnetic phases are VO_2–Co and V_2O_3–Co. But here one has to elucidate if these phases are really present (by high-resolution XPS recorded with good statistics, to be able to investigate photoelectrons coming from the bulk) and why they are antiferromagnetic coupled in the zero applied field. Magnetisation cycles such as the one exhibited by sample VO_2 (Figure 7(b)) may be a good starting point for magnetic field sensing and various kinds of actuators. (2) Another study that has to be performed is to investigate the metal–insulator transition in such materials and to correlate this transition with the evolution of magnetic properties. (3) Also, a more strict correlation between the oxygen vacancies found here by both XPS and XANES and the occurrence of ferromagnetism has to be carried out in order to discriminate between various processes contributing to the observed magnetic behaviour.

Nevertheless, we may end with confidence that the present study opens a new topic in the actual area of DMS.

Acknowledgements

This work was supported by the Romanian National Authority for Scientific Research under contract CNCSIS-PCCE ID-76. We acknowledge the valuable help of the Hasylab beamline scientist Dr Edmund Welter.

References

[1] H. Munekata, H. Ohno, S. Von Molnar, A. Segmuller, L.L. Chang, and L. Esaki, *Diluted magnetic III-V semiconductors*, Phys. Rev. Lett. 63 (1989), pp. 1849–1852; H. Ohno, *Making nonmagnetic semiconductors ferromagnetic*, Science 281 (1998), pp. 951–956; T. Jungwirth, J. Sinova, J. Masek, J. Kucera, and A.H. MacDonald, *Theory of ferromagnetic (III, Mn)V semiconductors*, Rev. Mod. Phys. 78 (2006), pp. 809–864.

[2] T. Dietl, H. Ohno, F. Matsukura, J. Cibert, and D. Ferrand, *Zener model description of ferromagnetism in zinc-blende magnetic semiconductors*, Science 287 (2000), pp. 1019–1022.

[3] M.A. Ruderman and C. Kittel, *Indirect exchange coupling of nuclear magnetic moments by conduction electrons*, Phys. Rev. 96 (1954), pp. 99–102; T. Kasuya, *A theory of metallic ferro- and antiferromagnetism on Zener's model*, Progr. Theor. Phys. 16 (1956), pp. 45–57; K. Yosida, *Magnetic properties of Cu-Mn alloys*, Phys. Rev. 106 (1957), pp. 893–898; E.V. Macocian and

S. Filip, *Spin wave spectrum in disordered Heisenberg spin systems*, J. Optoelectron. Adv. Mater. 8 (2006), pp. 1098–1104; D.J. Priour Jr, and S. Das Sarma, *Phase diagram of the disordered RKKY model in dilute magnetic semiconductors*, Phys. Rev. Lett. 97 (2006), pp. 127201(1–4); G. Tang and W. Nolting, *Carrier-induced ferromagnetism in diluted local-moment systems*, Phys. Rev. B 75 (2007), pp. 024426(1–5); E.Z. Meilikhov, *Diluted magnetic semiconductors with correlated impurities: Mean-field theory with RKKY interaction*, Phys. Rev. B 75 (2007), pp. 045204(1–11).

[4] J.M.D. Coey, M. Venkatesan, and C.B. Fitzgerald, *Donor impurity band exchange in dilute ferromagnetic oxides*, Nature Mater. 4 (2005), pp. 173–179.

[5] H. Ohno, D. Chiba, F. Matsukura, T. Omiya, E. Abe, T. Dietl, Y. Ohno, and K. Ohtani, *Electric-field control of ferromagnetism*, Nature 408 (2000), pp. 944–946; A. Oiwa, T. Slupinski, and H. Munekata, *Control of magnetization reversal process by light illumination in ferromagnetic semiconductor heterostructure p-(In, Mn)As/GaSb*, Appl. Phys. Lett. 78 (2001), pp. 518–520; H. Boukari, P. Kossacki, M. Bertolini, D. Ferrand, J. Cibert, S. Tatarenko, A. Wasiela, J.A. Gaj, and T. Dietl, *Light and electric field control of ferromagnetism in magnetic quantum structues*, Phys. Rev. Lett. 88 (2002), p. 207204(1–4).

[6] A. Sugawara, H. Kasai, A. Tonomura, P.D. Brown, R.P. Campion, K.W. Edmonds, B.L. Gallagher, J. Zemen, and T. Jungwirth, *Domain walls in the (Ga, Mn)As diluted magnetic semiconductor*, Phys. Rev. Lett. 100 (2008), pp. 047202(1–4).

[7] K.R. Kittilstved and D.R. Gamelin, *Activation of high-T-c ferromagnetism in Mn^{2+}-doped ZnO using amines*, J. Am. Chem. Soc. 127 (2005), pp. 5292–5293; K.R. Kittilstved, N.S. Norberg, and D.R. Gamelin, *Chemical manipulation of High-T-C ferromagnetism in ZnO diluted magnetic semiconductors*, Phys. Rev. Lett. 94 (2005), pp. 147209(1–4).

[8] R.J.O. Mossanek and M. Abbate, *Importance of the V 3d–0 2p hybridization in the Mott-Hubbard material V_2O_3*, Phys. Rev. B 75 (2007), pp. 115110(1–5).

[9] S. Ilani, A. Yacoby, D. Mahalu, and H. Shtrikman, *Microscopic structure of the metal-insulator transition in two dimensions,* Science 292 (2001), pp. 1354–1357; V.Y. Butko and P.W. Adams, *Quantum metallicity in a two-dimensional insulator*, Nature 409 (2001), pp. 161–164.

[10] M.W. Haverkort, Z. Hu, A. Tanaka, W. Reichelt, S.V. Streltsov, M.A. Korotin, V.I. Anisimov, H.H. Hsieh, H.J. Lin, C.T. Chen, D.I. Khomskii, and L.H. Tjeng, *Orbital-assisted metal-insulator transition in VO_2*, Phys. Rev. Lett. 95 (2005), pp. 196404(1–4); M. Demeter, M. Neumann, and W. Reichelt, *Mixed-valence vanadium oxides studied by XPS*, Surf. Sci. 454 (2000), pp. 41–44; K. Nagashima, T. Yanagida, H. Tanaka, and T. Kawai, *Stress relaxation effect on transport properties of strained vanadium dioxide epitaxial thin films*, Phys. Rev. B 74 (2006), pp. 172106(1–3); K. Nagashima, T. Yanagida, H. Tanaka, and T. Kawai, *Influence of ambient atmosphere on metal-insulator transition of strained vanadium dioxide ultrathin films*, J. Appl. Phys. 101 (2006), pp. 026103(1–4); H.T. Kim, Y.W. Lee, B.J. Kim, B.G. Chae, S.J. Yun, K.Y. Kang, K.J. Han, K.J. Yee, and Y.S. Lim, *Monoclinic and correlated metal phase in VO_2 as evidence of the Mott transition: Coherent phonon analysis*, Phys. Rev. Lett. 97 (2006), pp. 266401(1–4).

[11] A. Cavalleri, H.H.W. Chong, S. Fourmaux, T.E. Glover, P.A. Heimann, J.C. Kiefer, B.S. Mun, H.A. Padmore, and R.W. Schoenlein, *Picosecond soft X-ray absorption measurement of the photoinduced insulator-to-metal transition in VO_2*, Phys. Rev. B 69 (2004), pp. 1531006(1–4); A. Cavalleri, Th. Dekorsy, H.H.W. Chong, J.C. Kieffer, and R.W. Schoenlein, *Evidence for a structurally-driven insulator-to-metal transition in VO_2: A view from the ultrafast timescale,* Phys. Rev. B 70 (2004), pp. 161102(1–4).

[12] J. Zhang, R. Skomski, Y.F. Lu, and D.J. Sellmyer, *Temperature-dependent orbital-moment anisotropy in dilute magnetic oxides*, Phys. Rev. B 75 (2007), pp. 214417(1–5).

[13] D. Luca, D. Macovei, and C.M. Teodorescu, *Characterization of titania thin films prepared by reactive pulsed-laser ablation*, Surf. Sci. 600 (2006), pp. 4342–4346.

[14] C.M. Teodorescu, J.M. Esteva, R.C. Karnatak, and A. El Afif, *An approximation of the Voigt I profile for the fitting of experimental X-ray absorption data*, Nucl. Instrum. Methods Phys. Res. A 345 (1994), pp. 141–147.

[15] D. Mardare, D. Luca, C.M. Teodorescu, and D. Macovei, *On the hydrophilicity of TiO_2 thin films increased by nitrogen doping,* Surf. Sci. 601 (2007), pp. 4515–4520; D. Luca, C.M. Teodorescu, R. Apetrei, D. Macovei, and D. Mardare, *Preparation and characterization of increased-efficiency photocatalytic $TiO_{2-x}N_x$ thin films,* Thin Solid Films 515 (2007), pp. 8605–8610.

[16] J.F. Moulder, W.F. Stickle, P.E. Sobol, and K. Bomben, in *Handbook of X-ray Photoelectron Spectroscopy*, 2nd ed., J. Chastain, ed., Perkin-Elmer Corporation (Physical Electronics), Eden Prairie, MN, 1992.

[17] B.V. Crist, *Handbook of Monochromatic XPS Spectra, Volume 1: The Elements and Native Oxides and Volume 2: Commercially Pure Binary Oxides*, XPS International Inc., Mountain View, CA, 2004.

[18] S. Hüfner, *Photoelectron Spectroscopy: Principles and Applications*, 3rd ed., Springer, Berlin, 2003.

[19] S.L.T. Andersson and R.F. Howe, *An X-ray photoelectron study of metal clusters in zeolites*, J. Phys. Chem. 93 (1989), pp. 4913–4920.

[20] N.S. McIntyre, D.D. Johnston, L.L. Coatsworth, R.D. Davidson, and J.R. Brown, *X-ray photoelectron spectroscopic studies of thin-film oxides of cobalt and molybdenium*, Surf. Interf. Anal. 15 (1990), pp. 265–272.

[21] T.J. Chuang, C.R. Brundle, and D.W. Rice, *Interpretation of the X-ray photoemission spectra of cobalt oxides and cobalt oxide surfaces*, Surf. Sci. 59 (1976), pp. 413–429.

[22] B.J. Tan, K.J. Klabunde, and P.M.A. Sherwood, *XPS studies of solvated metal atom dispersed catalysts - evidence for layered cobalt manganese particles on alumina and silica*, J. Am. Chem. Soc. 113 (1991), pp. 855–861.

[23] C.D. Wagner, L.E. Davis, M.V. Zeller, J.A. Taylor, R.M. Raymond, and L.H. Gale, *Empirical atomic sensitivity factors for quantitative analysis by electron spectroscopy for chemical analysis*, Surf. Interf. Anal. 3 (1981), pp. 211–225.

[24] D. Mardare, V. Nica, C.M. Teodorescu, and D. Macovei, *Fe-doped TiO_2 thin films*, Surf. Sci. 601 (2007), pp. 4479–4483.

[25] B. Sass, C. Tusche, W. Felsch, F. Bertran, F. Fortuna, P. Ohresser, and G. Krill, *Magnetic and electronic interaction effects at the interfaces of Fe/V_2O_3 and Co/V_2O_3 bilayers*, Phys. Rev. B 71 (2005), pp. 014415(1–10).

[26] B.K. Teo, *EXAFS: Basic Principles and Data Analysis*, Springer, Berlin, 1983.

[27] J.J. Krebs, C. Vittoria, B.T. Jonker, and G.A. Prinz, *Magnetic resonance investigations of MBE-grown Fe/Ag/Fe sandwiches*, J. Magn. Magn. Mater. 54–57 (1986), pp. 811–813; G.A. Prinz, *Hybrid ferromagnetic-semiconductor structures*, Science 250 (1990), pp. 1092–1097.

[28] C. Kittel, *Introduction to Solid State Physics*, 4th ed., Wiley, New York, 1971.

[29] C.M. Teodorescu, F. Chevrier, R. Brochier, C. Richter, O. Heckmann, V. Ilakovac, P. De Padova, and K. Hricovini, *X-ray magnetic circular dichroism, photoemission and RHEED studies of Fe/InAs(100) interfaces,* Surf. Sci. 482 (2001), pp. 1004–1009; C.M. Teodorescu, F. Chevrier, R. Brochier, C. Richter, V. Ilakovac, O. Heckmann, P. De Padova, and K. Hricovini, *Reactivity and magnetism of Fe/InAs(100) interfaces,* Eur. Phys. J. B 28 (2002), pp. 305–313; C.M. Teodorescu and D. Luca, *Comparative study of magnetism and interface composition in Fe/GaAs(100) and Fe/InAs (100s)* Surf. Sci. 600 (2006), pp. 4200–4204.